Nanostructured Ni–P–TiO$_2$ composite coatings for electrocatalytic oxidation of small organic molecules

A. Abdel Aal [a,*], Hanaa B. Hassan [b], M.A. Abdel Rahim [b]

[a] Surface Protection and Corrosion Control Lab, Central Metallurgical Research and Development Institute, CMRDI, P.O. 87 Hellwan, Cairo, Egypt
[b] Department of Chemistry, Faculty of Science, Cairo University, Giza, Egypt

ABSTRACT

Ni–P–TiO$_2$ nanocomposite coatings with various contents of TiO$_2$ nano-particulates were prepared by electroless technique from Ni–P plating bath containing TiO$_2$ powder. X-ray diffractometer (XRD) and energy dispersive X-ray (EDX) technique have been applied in order to investigate the chemical composition and phase structure of the coatings, respectively. The incorporation of TiO$_2$ nano-particulates was found to be improved by the addition of TiO$_2$ powder to the plating bath. However, it has no significant effect on the wt% of P content in the deposit. Scanning electron microscope (SEM) images showed that the morphology of Ni–P–TiO$_2$ nanocomposite coating is finer and smoother than that of Ni–P coating. The catalytic activity of the prepared electrodes toward electro-oxidation of small organic molecules was studied and their stability with time was investigated. The catalytic activity was found to vary with the amount of the TiO$_2$ embedded into the Ni deposit.

© 2008 Elsevier B.V. All rights reserved.

1. Introduction

Autocatalytic electroless plating technology has been invented in 1946 [1]. From 1960's onwards, major progress in the field of electroless nickel polyalloy deposits and electroless composite coatings being tailored more closely to customer and environmental requirements [2]. Recently, electroless plating method has attracted a lot of interest not only in nano-fabrications, optics, and decoration but also in modifying the surface of various materials, such as non-conductors, semiconductors and metals [3–7].

Electroless nanometer composite coatings where nano-particulates used as reinforcing phase are important due to their excellent performance. The incorporation of nano-sized particles within Ni–P autocatalytic coatings greatly improved their properties and added entirely new features to the coatings performance, which enhanced their applicability in different industries such as electronic components and computers, general mechanics, automobile, paper mills, textile and food [8].

Particle-reinforced composite coatings could be fabricated previously by our group through the co-depositing of different particulate materials such as SiC, TiC/Al$_2$O$_3$, WC, Al$_2$O$_3$, AlN and polymers such as polytetrafluoroethylene and polyethylene [9–14]. Among these particulate, TiO$_2$ has attracted tremendous interest in re-

search community due to its wide application in engineering materials [15]. However, little attention has been paid to the incorporation of TiO$_2$ nano-particulates in Ni matrix; so far no work has been reported on the application of Ni–P–TiO$_2$ nanocomposite coatings for fuel cell applications.

Recently, nickel based electrodes have gained considerable interest in the electrochemical oxidation of small organic molecules [16,17]. Their electrocatalytic activities depend mainly on the catalytic role of Ni(OH)$_2$/NiOOH redox couple. Furthermore, TiO$_2$ and Ti coated with oxides of several other metals; Pt, Au, Fe, Co, Ni, Mo, Mn, Cr, Cu and Hg or their combinations Sb–Sn, Co–Mn, Ni–Si, Ni–Cr–Mo and Fe–Cr are used for methanol electro-oxidation [18,19]. A 50–50 ordered Ni–Ti alloy was found to be more active than Ni or Ti electrodes for methanol oxidation in acidic medium due to the formation of a passivating layer, which suppresses the nickel corrosion [20]. Thin films Ni–Ti (<100 nm) were prepared by ion-implanting was shown to be redox active and to promote the electrocatalytic oxidation of glucose in NaOH depending on the surface of Ni–Ti composition. Compared to the Ni–Ti bulk alloy (55.92:44.08), the Ni-implanted Ti displayed a more efficient catalytic activity and improved corrosion resistance [21].

The aim of the present work is to prepare Ni–P–TiO$_2$ nanocomposite coatings with different contents of TiO$_2$ particles onto the surface of commercial carbon using electroless deposition technique and to apply these electrodes for the electro-oxidation of small organic molecules such as methanol, formaldehyde, and

* Corresponding author. Tel.: +20 122690782; fax: +20 225010639.
E-mail addresses: foralsayed@gmail.com (A. Abdel Aal), hanaa20055@hotmail.com (H.B. Hassan).

glucose. The catalytic activity of the prepared electrodes toward electro-oxidation of small organic molecules and their stability with time has been investigated.

2. Experimental

2.1. Materials

The titanium dioxide, TiO_2, used in this work (Degussa P-25 anatase) with 25–40 nm was obtained from Degussa Company, Ridgefield Park, NJ. Commercial carbon was used as substrate for the electroless deposition. Chemicals were obtained from BDH (NaOH, glucose, methanol, formaldehyde AR) and were used without further purification and solutions were prepared using triply distilled water.

2.2. Plating procedures

Ni–P–TiO_2 nanocomposite coatings were deposited from a suspension of TiO_2 particles in a plating solution. Electroless nickel bath was used for preparing the Ni–P and Ni–P–TiO_2 composite coatings. The plating bath consists of nickel sulfate 35 g/L as a source of nickel, sodium hypophosphite 15 g/L as reducing agent, and sodium citrate 15 g/L, sodium acetate 5 g/L as a complexing agent to control the free nickel ions in the plating solution and deposition rate. The bath operated at pH 4.7–4.9 and temperature 90 ± 2 °C. The TiO_2 particles were added to the solution from 1 to 5 g/L. Magnetic stirring was applied to mix the TiO_2 particles and the electrolyte for 8 h for complete dispersion of powder into plating solution. Subsequently, the suspension was stirred by ultrasonic agitation for 30 min just before plating.

The Ni–P–TiO_2 nanocomposite coatings of about 10 μm in thickness were deposited on commercial carbon rod of 0.125 cm^2 apparent surface area using nickel plate as an anode. The bath was stirred by a magnetic stirrer (150 rpm) in the plating process. Pure Ni–P coatings were also obtained under the same condition from an electrolyte without TiO_2 particles. After plating, the specimens were taken out then thoroughly rinsed with deionized water and air dried at room temperature. Then, these specimens were used for electro-oxidation measurements without any further treatments.

Zeta potential measurements were carried out using Lazer Zeta meter Malven Instrument (Zeta sizer 2000). Ground sample (0.02 g) was immersed in total volume of 50 ml of electroless plating solution. pH was adjusted at desired value using NaOH and HCl solution. The samples were shaked for 30 min then the zeta potential was measured. Surface areas of the prepared electrodes were recorded using Nova 2000 series based on the well-known Brunauer, Emmett and Teller (B.E.T.) theory.

2.3. Electrochemical measurements

Electrochemical measurements were performed on the prepared electrodes of a disc shaped each of a surface area of 0.125 cm^2. The surface area was calculated from the apparent area and the current density was referred to it. A conventional three-electrodes glass cell with a Pt sheet as a counter electrode and Hg/HgO/1.0 M NaOH (MMO, E^0 = 140 mV vs. NHE) as a reference electrode were used. All experiments were carried out at room temperature of 30 ± 2 °C. The electrochemical measurements were performed using an Amel 5000 system (supplied by Amel instrument, Italy) driven by a PC for data processing. The PC was interfaced with the instrument through a serial RS-232 C card. Amel Easy Scan software was used in connection with the PC to control the Amel 5000 system.

The phase structure of the composite coatings was studied by X-ray diffractometry (BRUKER axc-D8) using Cu Kα radiation with λ = 0.1542 nm. The surface morphology of the coatings was observed using a scanning electron microscopy (JEOL-JSM-5410) and the percentage of co-deposited TiO_2 particles was evaluated by using energy dispersive X-ray spectroscopy (EDX-Oxford) analysis tool.

3. Results and discussion

3.1. Characterization of Ni–P–TiO_2 nanocomposite coatings

Ni–P–TiO_2 composite coating was prepared onto the carbon substrate surface from a suspension of TiO_2 particles in aqueous bath by electroless plating technique. Generally, the structure and properties of electroless Ni–P coating depend mainly on the amount of phosphorus present in the deposit. The surface composition of the coating was determined by energy dispersive X-ray spectroscopy (EDX). In each measurement, an area of 10 μm in diameter was examined to a depth of about 2 μm. In other words, EDX analysis has been carried out to determine the influence of co-deposition of TiO_2 particles on the chemical composition of the coating (Fig. 1). The chemical compositions of as-plated Ni–P and composite coatings prepared with different contents of TiO_2 powder in plating bath are given in Table 1. For Ni–P coating, the wt% of P content was 5.3 wt% referring to the low P content. With TiO_2 addition (0–5 g/L), marginal variation in phosphorus content was noticed (5.3–5.6 wt%). On the other hand, increasing in TiO_2 powder content (1–3 g/L) enhances the wt% of co-deposited TiO_2 in the coatings (1.4–4.5 wt%). However, further increase in powder addition has a slight effect on the incorporation process.
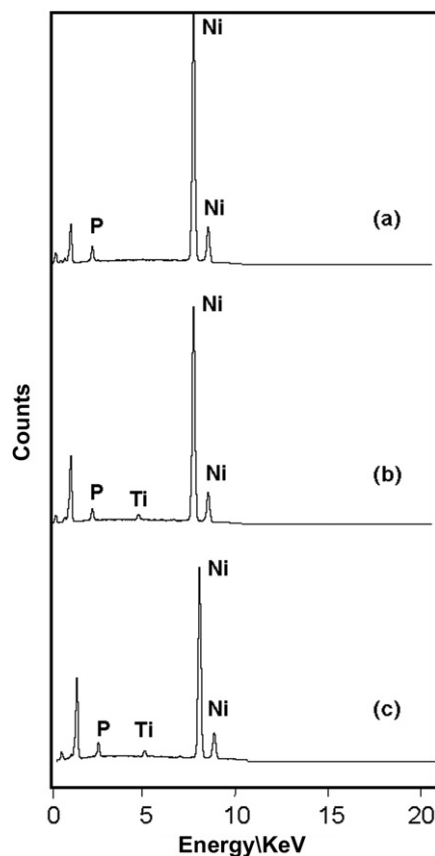

Fig. 1. EDX analysis for: (a) Ni–P, (b) Ni–P–TiO_2 (I), and (c) Ni–P–TiO_2 (II) coatings.

Table 1
Effect of TiO$_2$ concentration in the electrolyte on the composition of deposit

Electrode structure	TiO$_2$ content in bath (g/l)	Coating composition		
		Ni (wt%)	P (wt%)	TiO$_2$ (wt%)
Ni–P/C	0	94.7	5.3	–
Ni–P–TiO$_2$/C (I)	1	92.4	5.5	1.4
Ni–P–TiO$_2$/C (II)	3	90.1	5.4	4.5
Ni–P–TiO$_2$/C (III)	5	89.3	5.6	5.1

The co-deposition process can be ascribed probably to the electrostatic absorption of Ni ions onto the inert particles of TiO$_2$ [15,21]. Fig. 2 shows the variation of zeta potential of TiO$_2$ with pH of the Ni–P bath. It is evident that within the scale of pH value (2–12), the zeta potential was always negative. The negative zeta potential of TiO$_2$ particles is an effective factor in the trapping of Ni ions onto the surface of powder particles in the plating bath of a pH value 5. Hence, the amount of adsorbed Ni^{2+} ions on the surface of TiO$_2$ particles increases with an increase in TiO$_2$ content in the bath. Beside the effects of ion adsorption, agitation has been shown to play a significant role in the increasing of physical collisions of particles with the substrate surface, encapsulating and incorporating the TiO$_2$ particles into deposit in the mechanical locks of the coating [15,22].

SEM surface morphology of the pure Ni–P and Ni–P–TiO$_2$ coatings containing different contents of TiO$_2$ particles is shown in Fig. 3. It can be observed that the Ni–P–TiO$_2$ nanocomposite coatings show a smooth and fine surface compared with Ni–P coating. Fig. 4 presents XRD patterns of the Ni–P and composite coatings containing different TiO$_2$ contents. Diffraction pattern of Ni–P (blank) shows a single broad peak at around 45° characteristic of amorphous state with preferred orientation of Ni(1 1 1) and the area of amorphous state is very wide.

The grain size (t) of Ni–P and Ni–P–TiO$_2$ coatings can be estimated by the Scherrer equation [23]:

$$t = \frac{0.9\lambda}{B\cos(\theta_B)} \tag{1}$$

where λ is Cu (Kα) wavelength, B is the broadening of the full width at half maximum (F.W.H.M) and θ_B is the Bragg's angle. The calculated grain size using Scherrer method is around 1.9 nm for Ni–P. The phase composition investigations of Ni–P–TiO$_2$ coatings reveal the presence of two phases (Fig. 4). Apart from single broad peak corresponds to amorphous Ni(1 1 1) plane at 45°, there are low intensity peaks characterized for TiO$_2$. The calculated grain sizes
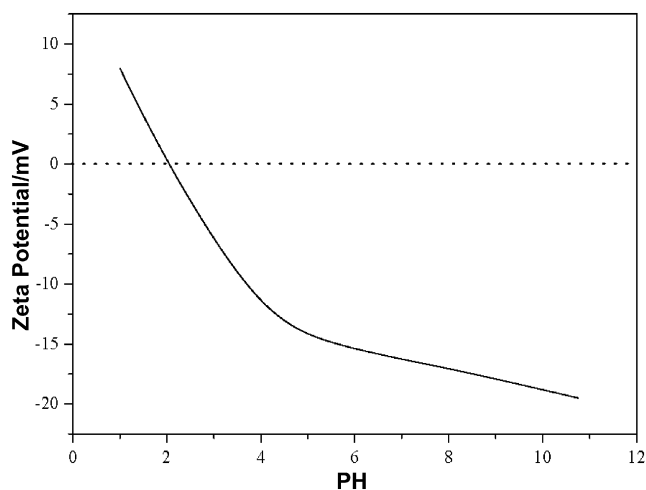

**Fig. 2.** The variation of zeta potential of TiO$_2$ particles with pH.

from the Scherrer formula for the diffracted peak of Ni for Ni–P and N–P–TiO$_2$ coatings are summarized in Table 2. The data indicated that the size of Ni grains of the Ni–P–TiO$_2$ nanocomposite coating is smaller than that of Ni–P coating. Such decrease in grain size can be attributed to the distribution of TiO$_2$ nano-particulates on the boundaries of Ni grains, which restricts the growth of Ni grains in the deposition process and results in the fine and smooth surface [24].

3.2. Electro-oxidation of small organic molecules

The electrochemical behavior of the prepared electrodes was studied in NaOH solution in order to study the electro-oxidation of small organic molecules such as methanol, glucose and formaldehyde. First, the cyclic voltammetric behavior of Ni–P/C electrode in 0.5 M NaOH solution is shown in Fig. 5. The polarization was started at a scan rate of 50 mV/s from −1200 to +1500 mV (MMO) in the anodic direction and then the scan was reversed in the cathodic direction back to −1200 mV. The hydrogen evolution takes place at the starting potential at high cathodic current, while the oxygen evolution can be observed at relatively high positive potential. Additionally, two small peaks are observed in the blank voltammogram, one in the anodic direction at about +500 mV (MMO) due to the formation of NiOOH (Fig. 5) and the other in the cathodic direction at about +450 mV due to the reduction of NiOOH to Ni(OH)$_2$ [25,26]:

$$Ni(OH)_2 + OH^- = NiOOH + H_2O + e^- \tag{I}$$
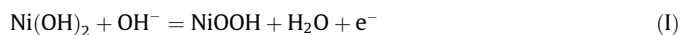
Addition of 2.0 M methanol to the electrolyte changes the voltammetric response of the electrode. The solid line in Fig. 5 represents the electrochemical oxidation of 2.0 M methanol in 0.5 M NaOH at the same scan rate. The oxidation process was started at +500 mV (MMO) with gradual increase in the oxidation current density reached its maximum value of 57 mA cm^{-2} at about +919 mV in the anodic direction. Then, the scan was reversed and another reoxidation peak appeared in the reverse scan at the same potential value probably due to the oxidation of the adsorbed methanol and/or the intermediate product of methanol oxidation. Adsorbed CO is one of the most known intermediate products of methanol oxidation, which causes deactivation and blocking of the active sites of the electrode surface during the oxidation process with the time [27]. On the other hand, formate and CO$_2$ were identified as the main solution reaction products in NaOH solution [28]. It was found that the presence of oxide, hydroxide and/or oxyhydroxide groups is an essential for the electro-oxidation of organic compound demands [29]. On the Ni–P/C electrode, the methanol oxidation process starts at a potential value corresponding to the formation of NiOOH species as shown from the Fig. 5. It can be proposed that methanol is oxidized on the Ni–P/C electrode through the reaction with NiOOH, i.e. NiOOH acts as electron transfer mediator for the oxidation process [30–32]:

$$NiOOH + methanol \leftrightarrow Ni(OH)_2 + products \tag{II}$$
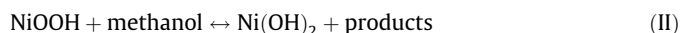
Electrochemical oxidation of glucose was also studied on Ni–P/C electrode in NaOH solution. Fig. 6 represents the cyclic voltammogram of Ni–P/C electrode in 0.5 M NaOH solution in absence and presence of glucose (0.1 M) at a scan rate of 50 mV/s. The same redox couples of Ni, i.e. (Ni^{3+}/Ni^{2+}) were appeared at +500 and +450 mV in both anodic and cathodic directions. The electro-oxidation of glucose was started at about +450 mV as NiOOH species are formed and the current density increased in the anodic direction reaching its maximum value of 55 mA cm^{-2} at potential of +860 mV. Then, the current density decreased whereas the scan is reversed and another reoxidation peak of glucose and/or the intermediate product of glucose oxidation appeared at the same potential value. Gluconic acid as the main reaction product in
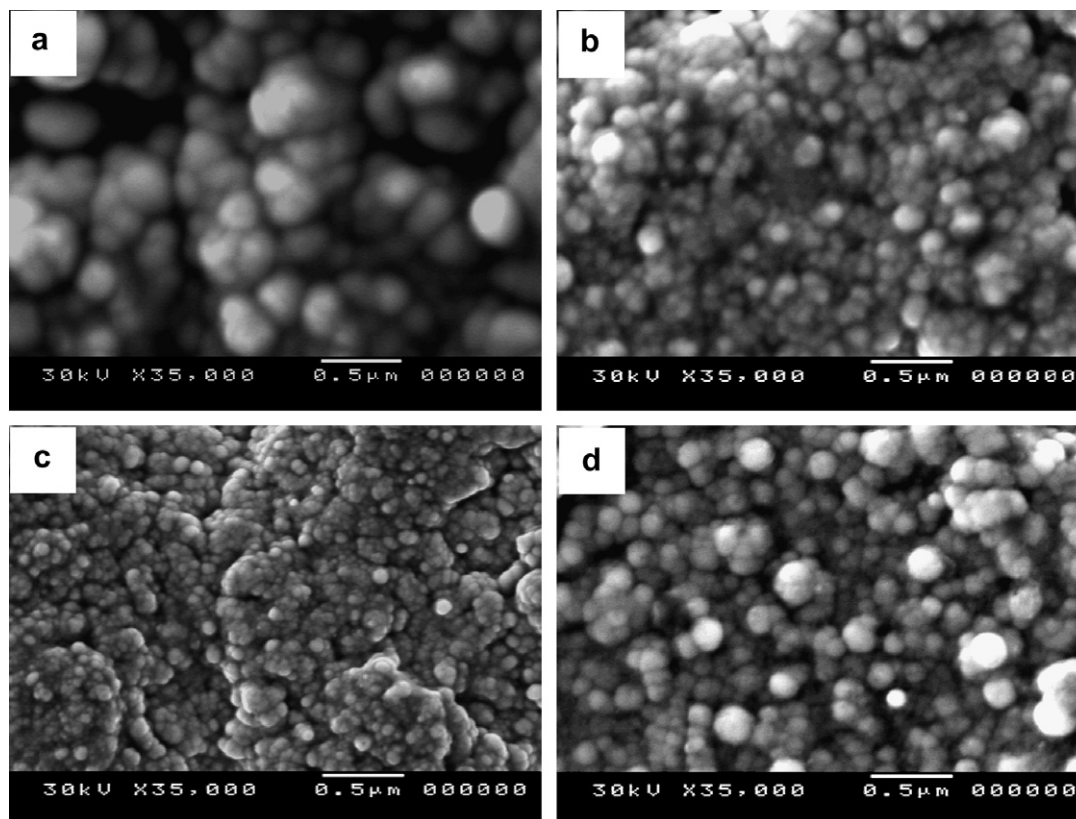
Fig. 3. SEM images of: (a) Ni–P and Ni–P–TiO$_2$ (b) I, (c) II, and (d) III coatings.
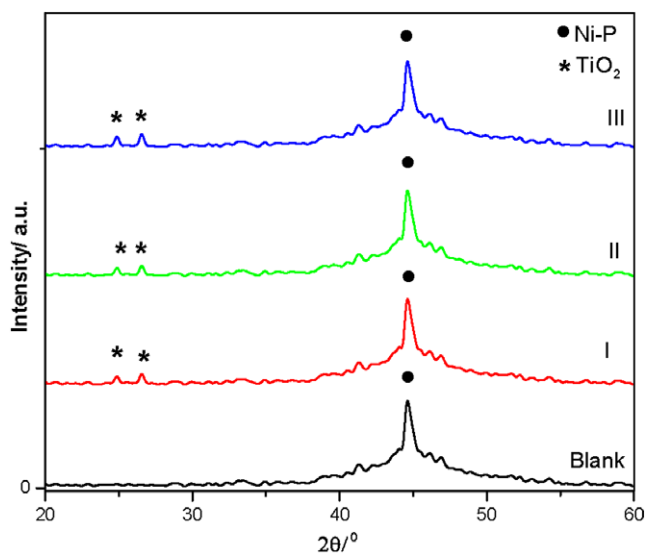

Fig. 4. XRD of the prepared electrodes (I, II, III) in comparison with Ni–P/C electrode.

Table 2
Grain size and surface area of Ni(1 1 1) in the Ni–P and Ni–P–TiO$_2$ composite coatings

Samples	Grain size (nm)	Actual surface area (m^2/g)
Ni–P/C	1.90	25
Ni–P–TiO$_2$/C (I)	1.60	101
Ni–P–TiO$_2$/C (II)	1.30	143
Ni–P–TiO$_2$/C (III)	1.00	156

acidic and in neutral media beside many other carboxylic acids such as glucaric, glucuronic, tartaric, glyoxylic, oxalic, glycolic and formic acids were detected [33]. Accordingly, it is expected that the salts of these acids are formed in alkaline solution. Hence, the oxidation of glucose on the Ni–P/C electrode can be carried out through the reaction with NiOOH [30,31].

In addition, the electrochemical oxidation of formaldehyde was studied at Ni–P/C electrode. Fig. 7 represents the cyclic voltammograms of this electrode in 0.5 M NaOH at a scan rate of 50 mV/s in absence and in presence of 2.0 M HCHO. It is obvious that the oxidation process occurs with the formation of NiOOH species. The oxidation current density increases in the anodic direction reaching a high value at relatively high overpotential. Then, the scan was reversed and another reoxidation peak appeared in the negative scan due to the oxidation of the adsorbed formaldehyde and/or the intermediate product of formaldehyde oxidation. The oxidation current density is about 74 mA cm^{-2} at +1000 mV (MMO). The final products of HCHO oxidation is HCOO$^-$ and/or CO$_2$ depending on the type of the used electrode [34]. It can be mentioned that NiOOH is an electron transfer mediator for the oxidation of formaldehyde on the Ni–P/C electrode [30,31].

In a trial to increase the catalytic activity and the stability of the above used catalyst toward the electro-oxidation of small organic molecules, other electrodes with different contents of TiO$_2$ were prepared (Table 1). Three-electrodes named as (I, II, III) containing different TiO$_2$ contents of 1.4, 4.5 and 5.1 wt%, respectively were prepared. The electro-oxidation of methanol on the three Ni–P–TiO$_2$/C electrodes in 0.5 M NaOH solution was examined. Fig. 8a illustrates cyclic voltammograms of the three-electrodes (I, II and III) in 0.5 M NaOH as a blank solution at a scan rate of 50 mV/s from −1200–1500 mV (MMO). The shape of these cyclic voltammograms in 0.5 M NaOH is almost the same as the cyclic voltammogram pattern of Ni–P/C electrode (Fig. 5) in the same electrolyte
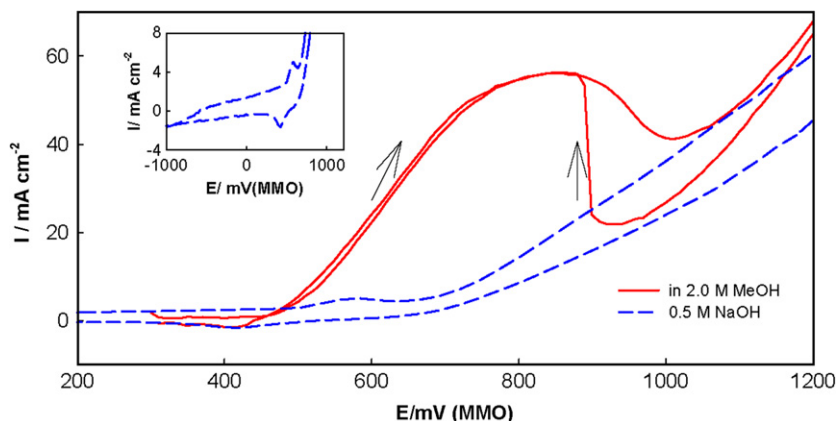
Fig. 5. Cyclic voltammograms of Ni–P/C electrode in 0.5 M NaOH (the dashed line) and in presence of 2.0 M MeOH (the solid line) at a scan rate of 50 mV/s (MMO).
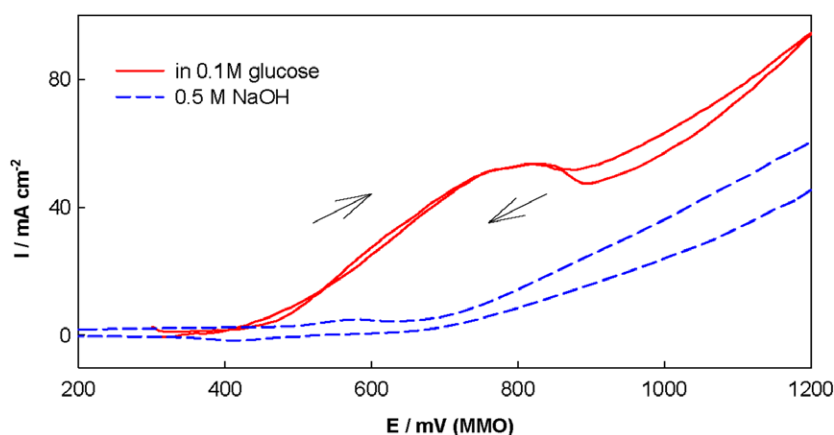

Fig. 6. Cyclic voltammograms of Ni–P/C electrode in 0.5 M NaOH (the dashed line) and in presence of 0.1 M glucose (the solid line) at a scan rate of 50 mV/s (MMO).
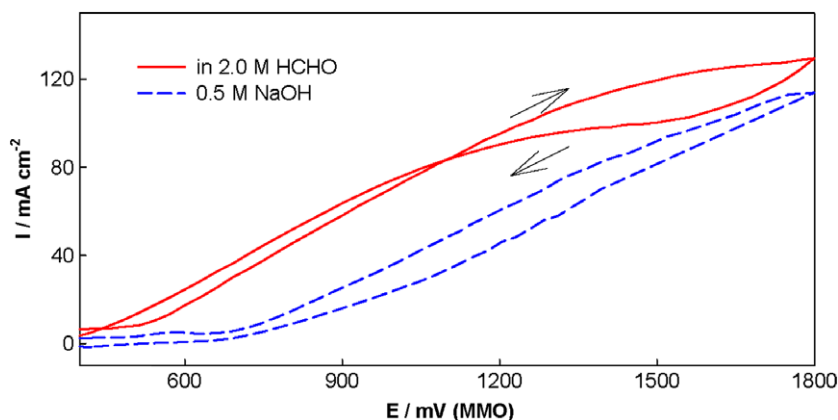

Fig. 7. Cyclic voltammogram of Ni–P/C electrode in 0.5 M NaOH in presence of 2.0 M HCHO at a scan rate of 50 mV/s (MMO).

with a few differences. It was found that, H_2 evolution peak appeared at the starting negative potential while the O_2 evolution peak appeared at more positive potential. The two peaks of Ni redox couples i.e., (Ni^{3+}/Ni^{2+}) appeared with higher peak current densities compared to that obtained with Ni–P/C electrode. Depending on the composition of the applied electrodes, the higher amount of TiO_2 in the prepared electrode, the higher height of the peak current densities of the redox couples. On the other hand, the potential of the anodic peak shifted towards the positive potential and that of the cathodic peak shifted towards the less positive one. It

can be observed that the presence of TiO_2 in the prepared electrode enhances the formation of Ni redox couple (Ni^{3+}/Ni^{2+}). Fig. 8b represents cyclic voltammograms of these electrodes in 0.5 M NaOH in presence of 2.0 M MeOH at a scan rate of 50 mV/s from 200 to 1500 mV (MMO). It was found that the oxidation process starts at +400 mV as NiOOH species is formed and the oxidation current density of methanol increases in the anodic direction up to +1500 mV. With reversing the scan down to +200 mV, another reoxidation process of the adsorbed methanol and/or its intermediate products takes place in the reverse scan. Since, the oxidation
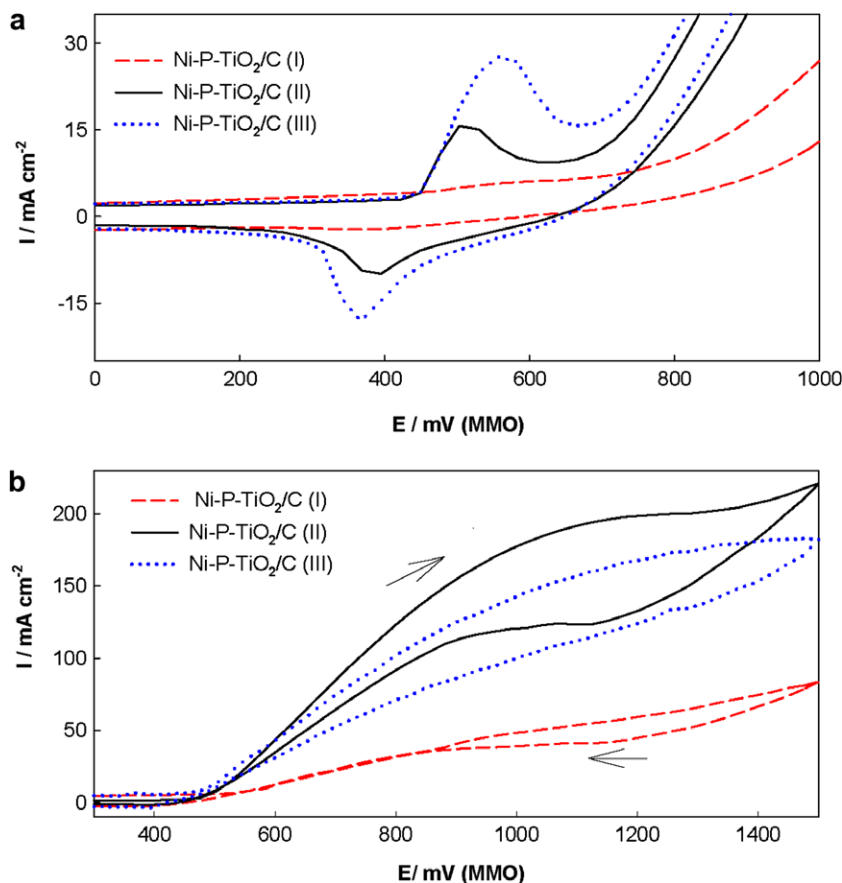
Fig. 8. (a) Cyclic voltammograms of Ni–P–TiO₂/C electrodes [I, II, III] in 0.5 M NaOH at a scan rate of 50 mV/s (MMO). (b) Cyclic voltammograms of Ni–P–TiO₂/C electrodes [I, II, III] in 0.5 M NaOH in presence of 2.0 M MeOH at a scan rate of 50 mV/s (MMO).

of methanol on the investigated electrodes is characterized by very broad peaks over wide range of potentials. It was necessary to measure and compare values of oxidation current density at a constant selected potential value (Table 3). The data indicates that as the TiO_2 content increases in the prepared electrodes, the oxidation current density increases and the modified electrode II with 4.5 wt% TiO_2 exhibited the highest oxidation current density value compared to the other two electrodes (I and III) at +919 mV as shown from Table 3. Besides, the oxidation current density of methanol at that electrode is much higher than that on Ni–P/C electrode at the same potential value (Table 3). For all the applied electrodes, the oxidation process starts only after the formation of NiOOH species as an electron transfer mediator [30].

Therefore, a conclusion can be drawn that Ni–P–TiO₂/C electrodes are superior to Ni–P/C electrode towards methanol electro-oxidation with respect to the oxidation current density. The catalytic activity improvement of Ni–P–TiO₂/C electrodes probably attributed to the presence of TiO_2 that enhances the formation of

Ni^{3+}/Ni^{2+} redox couple. The Ni^{3+} ions are considered the main species necessary for methanol oxidation on Ni electrodes in alkaline solution. Moreover, the presence of the mixed oxides (i.e., the nickel oxides and titanium oxides) may serve as good electron transfer mediators for the oxidation process [35]. In addition, the presence of TiO_2 reduces the particle size of Ni and increases the actual surface area improving the catalytic activity towards electro-oxdiation of small organic molecules by increasing the number of active sites [36]. However, the Ni–P–TiO₂/C with 4.5 wt% TiO_2 showed higher catalytic activity than that electrode III with 5.1 wt% TiO_2 due the lower Ni content in later electrode.

The chronoamperometric study in Fig. 9 represents the relation between the steady state current of methanol oxidation at the peak potential of +919 mV (MMO) and the time in minutes for the three-electrodes Ni–P/C, Ni–P–TiO₂/C (I) and Ni–P–TiO₂/C (II) respectively. It is seen that Ni–P–TiO₂/C electrodes (I, II) exhibited higher stability than that of Ni–P/C electrode. Since TiO_2 suppresses the deactivation of the electrode surface and improves the stability of these electrodes through complete oxidation of intermediate product of the oxidation process such as CO. Moreno et al. found that TiO_2 acts as a Pt protecting matrix in the hydrogen oxidation reaction, which increases CO oxidation [37,38]. Additionally, Mehandru et al. have proved that CO dissociates on Pt–Ti alloys much easier than on pure Pt [39].

In order to confirm the role of TiO_2 with Ni towards the enhancement of the electrocatalytic oxidation of small organic molecules such as methanol, similar electrode was prepared using Al_2O_3 in the same ratio instead of TiO_2. The bath composition and plating conditions for the preparation of Ni–P–Al₂O₃ composite coatings have been optimized and published elsewhere [40]. SEM

Table 3
The oxidation current densities of small organic molecules on different electrodes at constant potentials

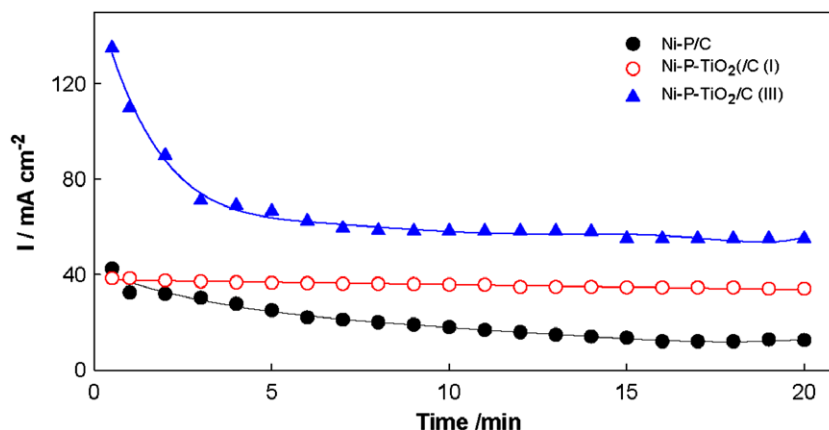| Electrode structure	Methanol I (mA cm⁻²) at +919 mV (MMO)	Glucose I (mA cm⁻²) at +860 mV (MMO)	Formaldehyde I (mA cm⁻²) at +1000 mV (MMO)
Ni–P/C	57	55	74
Ni–P–TiO₂/C (I)	44	41	55
Ni–P–TiO₂/C (II)	175	113	87
Ni–P–TiO₂/C (III)	130	78	67

Fig. 9. The steady state oxidation current density values of 2.0 M methanol in 0.5 M NaOH at a potential of +919 mV (MMO) with time in minutes.
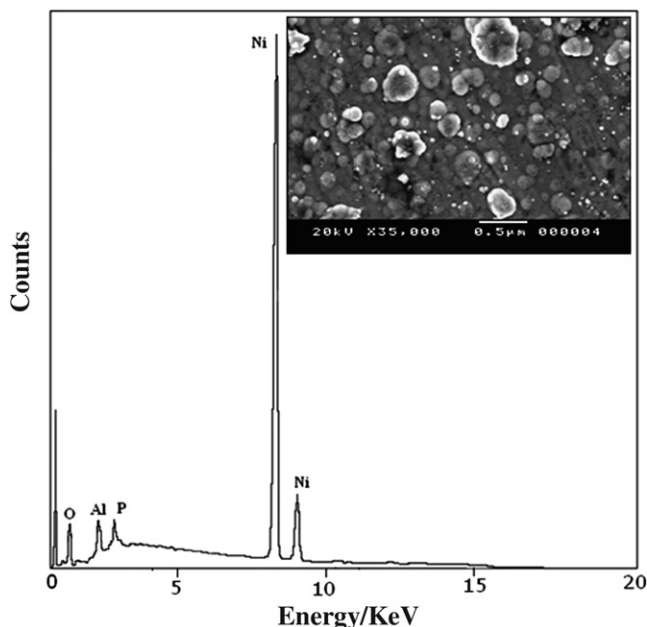

Fig. 10. EDX analysis and SEM pattern of Ni–P–Al$_2$O$_3$ coating.

micrograph in Fig. 10 shows the distribution of Al$_2$O$_3$ particles into the Ni–P deposit. It is obvious that the obtained composite layers have a mat-gray metallic surface of Ni–P with white spots visible to the naked eye of Al$_2$O$_3$. To further confirm the presence of the Al$_2$O$_3$ particles in the coating, EDX analysis of the surface has been carried out and the corresponding spectra is shown in Fig. 10. Al$_2$O$_3$ peak is observed other than nickel and phosphorous peaks. This confirms the presence of second phase Al$_2$O$_3$ particles in the Ni–P matrix.

The cyclic voltammogram of Ni–P–Al$_2$O$_3$/C (4.5 wt% Al$_2$O$_3$) was recorded in 0.5 M NaOH in absence and in presence of 2.0 M MeOH at a scan rate of 50 mV/s (Fig. 11). The shape of the blank cyclic voltammogram (the dashed line) almost the same as the cyclic voltammogram pattern of Ni–P/C electrode in the same electrolyte. However, the current densities of the redox couples of Ni (i.e., Ni^{3+}/Ni^{2+}) formed at +580 and +450 mV (MMO) are slightly smaller than that of Ni–P/C electrode. In addition, H$_2$ evolution peak appeared at more negative potential while the O$_2$ evolution peak detected at more positive one. It is clear in Fig. 11 that the oxidation peak current density of methanol at Ni–P–Al$_2$O$_3$/C (4.5 wt%) electrode is about 57 mA cm^{-2} at a potential of +919 mV (MMO), which is similar to that value obtained at Ni–P/C electrode without TiO$_2$. This clearly illustrates the specificity of TiO$_2$ in enhancement of the oxidation process.

Electrochemical oxidation of glucose was also studied on Ni–P–TiO$_2$/C electrodes (I, II, III) in 0.5 M NaOH solution. Fig. 12a demonstrates cyclic voltammograms of the three-electrodes in 0.5 M
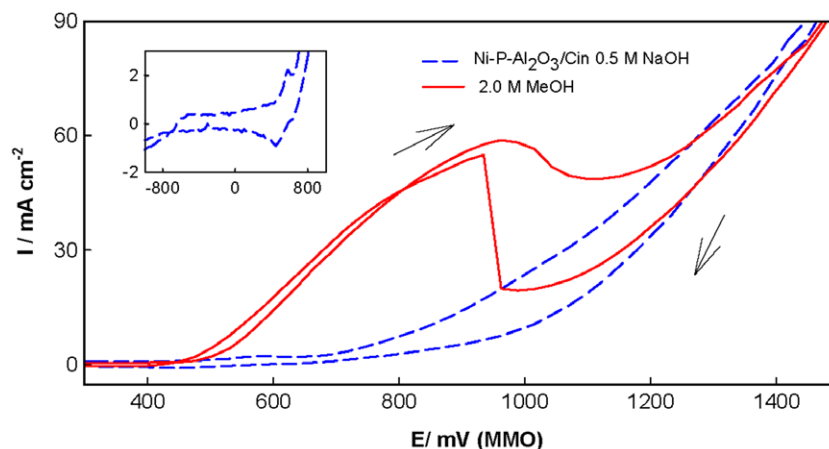

Fig. 11. Cyclic voltammograms of Ni–P–Al$_2$O$_3$/C electrode in 0.5 M NaOH (the dashed line) and in presence of 2.0 M methanol (the solid line) at a scan rate of 50 mV/s (MMO).
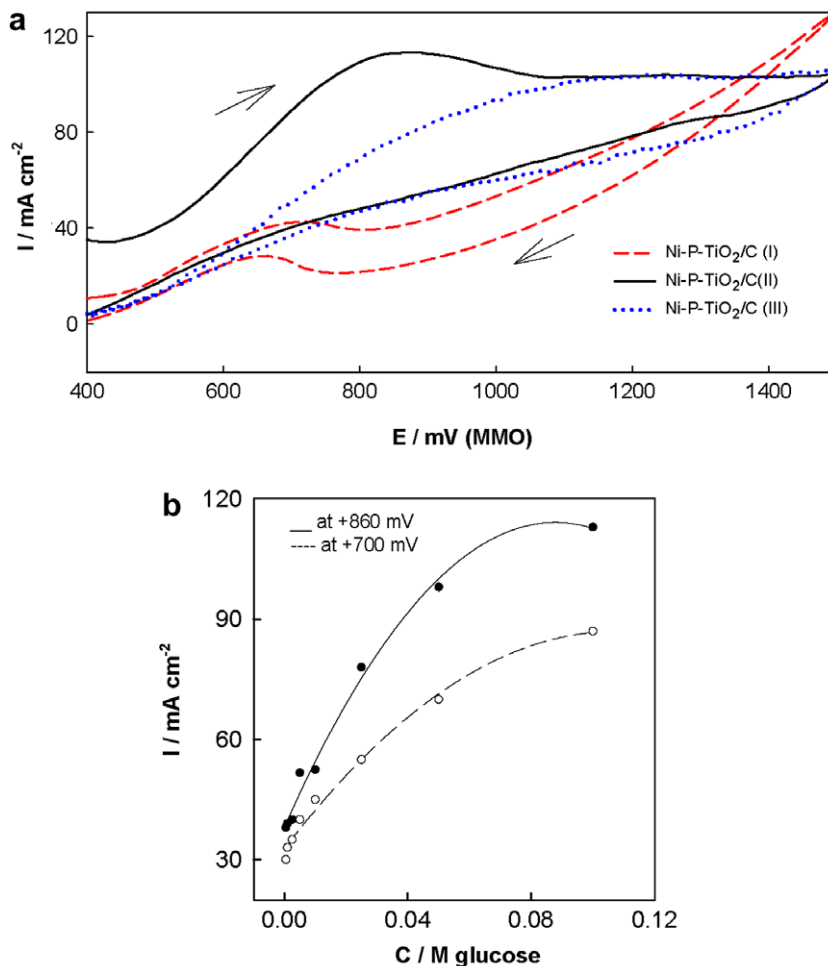
Fig. 12. (a) Cyclic voltammograms of Ni–P–TiO$_2$/C electrodes (I, II, III) in 0.5 M NaOH in presence of 0.1 M glucose a scan rate of 50 mV/s (MMO). (b) The relation between the concentration of glucose and the oxidation current density values at +860 mV (the solid line) and +700 mV (the dashed line) MMO at Ni–P–TiO$_2$/C (II).

NaOH in presence of 0.1 M glucose at a scan rate of 50 mV/s. The same redox couples of Ni appeared as stated above in the 0.5 M NaOH as a blank solution (Fig. 8a) and the electro-oxidation of glucose starts at +450 mV as NiOOH species formed and the current density increases in the anodic direction. Then, the current density decreases, whereas the scan is reversed and another oxidation peak appeared in the reverse scan at the same potential value

due to the oxidation of the glucose and/or the intermediates of the glucose oxidation process. Therefore, the Ni–P–TiO$_2$/C (II) showed the highest oxidation current density value of about 113 mA cm^{-2} at +860 mV (MMO) compared to the other two electrodes (Table 3).

In order to study the effect of glucose concentration at Ni–P–TiO$_2$/C (II) electrode, different glucose concentrations were pre-
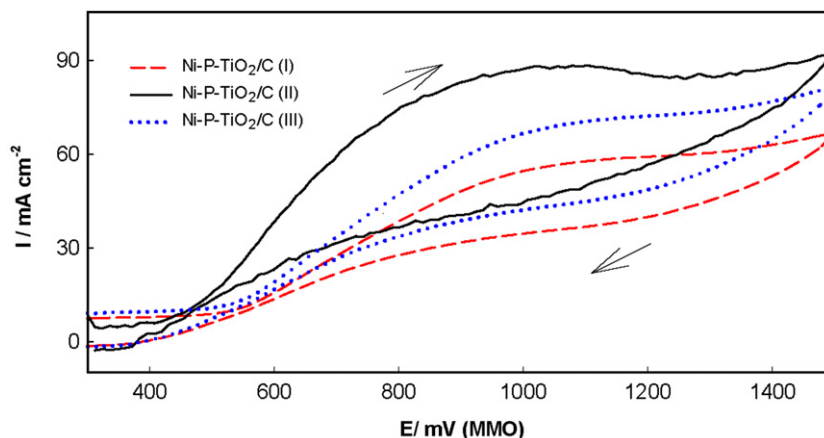

Fig. 13. Cyclic voltammograms of Ni–P–TiO$_2$/C electrodes [I, II, III] in 0.5 M NaOH in presence of 2.0 M HCHO at a scan rate of 50 mV/s (MMO).

pared in the range from 0.2 down to 0.0005 M in 0.5 M NaOH and the cyclic voltammograms were recorded at a scan rate of 50 mV/s. It was found that as the concentration of glucose increases, the oxidation current densities at +860 and +700 mV (MMO) increase (Fig. 12b).

Fig. 13 represents the cyclic voltammograms of electro-oxidation of 2.0 M HCHO in 0.5 M NaOH at a scan rate of 50 mV/s. As shown the oxidation process occurs at relatively lower over potentials compared to that occurs at Ni–P/C electrode. The data in Table 3 indicated that the Ni–P–TiO$_2$/C (II) exhibited the highest oxidation current density of 87 mA cm^{-2} compared to the other two electrodes.

4. Conclusions

It was feasible to prepare Ni–P–TiO$_2$ nanocomposite coating by properly incorporating TiO$_2$ nano-particulate to be co-deposited in the Ni–P plating bath. The content of TiO$_2$ particles in Ni–P–TiO$_2$ composite coatings increases with increasing concentration of TiO$_2$ in the plating bath. The nanocomposite Ni–P–TiO$_2$ coatings showed a smaller grain size compared with Ni–P coating. The nanocomposite Ni–P–TiO$_2$ exhibited higher catalytic activity towards the electrochemical oxidation of small organic molecules than Ni–P and the highest activity was exhibited by Ni–P–TiO$_2$ (4.5% TiO$_2$) electrode.

References

[1] G. Jiaqiang, L. Lei, W. Yating, S. Bin, H. Wenbin, Surf. Coat. Technol. 200 (2005) 5836.
[2] M. Ebrahimian-Hosseinabadi, K. Azari-Dorcheh, S.M. Moonir Vaghefi, Wear 260 (2006) 123.
[3] Z. Haijun, W. Xiangwei, J. Quanli, J. Xiaolin, Mater. Des. 28 (2007) 1369.
[4] C.A. Leon, R.A.L. Drew, J. Mater. Sci. 35 (2000) 4763.
[5] T. Kobayashi, J. Ishibashi, S. Mononobe, M. Ohtsu, H. Honma, J. Electrochem. Soc. 147 (2000) 1046.
[6] L.M. Ang, T.S.A. Hor, C.Q. Xu, C.H. Tung, S.P. Zhao, J. Wang, Carbon 38 (2000) 363.
[7] F.Z. Kong, X.B. Zhang, W.Q. Xiong, F. Liu, W.Z. Huang, Y.L. Sun, J. Tu, X.W. Chen, Surf. Coat. Technol. 155 (2002) 33.
[8] O.A. León, M.H. Staia, H.E. Hintermann, Surf. Coat. Technol. 200 (2005) 1825.
[9] A. Abdel Aal, K.M. Ibrahim, Z. Abdel Hamid, Wear 260 (2006) 1070.
[10] Z. Abdel Hamid, S.A. El Badry, A. Abdel Aal, Surf. Coat. Technol. 201 (2007) 5948.
[11] A. Abdel Aal, Z.I. Zaki, Z. Abdel Hamid, Mater. Sci. Eng. A 447 (2007) 87.
[12] A. Abdel Aal, M. Bahgat, M. Radwan, Surf. Coat. Technol. 201 (2006) 2910.
[13] Z. Abdel Hamid, A.M. Omar, Surfact. Detergent 6 (2003) 163.
[14] Z. Abdel Hamid, I.M. Ghayad, Mater. Lett. 53 (2002) 238.
[15] A. Abdel Aal, Mater. Sci. Eng. A 474 (2008) 181.
[16] M.A. Abdel Rahim, R.M. Abdel Hameed, M.W. Khalil, J. Power Source 134 (2004) 160.
[17] M.A. Abdel Rahim, R.M. Abdel Hameed, M.W. Khalil, J. Power Source 135 (2004) 42.
[18] G. Kokkinids, A. Papoutsis, D. Stoychev, A. Milchev, J. Electroanal. Chem. 486 (2000) 48.
[19] B.M. Lotvin, Yu.B. Vasil, Electrokimiya 16 (1980) 1419.
[20] R. Manoharan, J.B. Goodenough, J. Mater. Chem. 2 (1992) 875.
[21] S.G.J. Heijmand, H.N. Stein, Langmuir 11 (1995) 422.
[22] S.M. Monir Vaghefi, A. Saatchi, M. Ebrahimian-Hoseinabadi, Surf. Coat. Technol. 168 (2003) 259.
[23] B.D. Cullity, Elements of X-ray Diffraction, second ed., Addison Wesley Publishing, London, 1978.
[24] Yating Wu, Hezhou Liu, Bin Shen, Lei Liu, Wenbin Hu, Tribol. Int. 39 (2006) 553.
[25] M. Vukovic, J. Appl. Electrochem. 24 (1994) 878.
[26] G.R. Mundy, R.J. potter, P.A. Christensen, A. Hamnett, J. Electroanal. Chem. Interf. Electrochem. 279 (1990) 734.
[27] E. Morallon, J.F. Cases, J.L. Vazquez, A. Aldaz, Electrochim. Acta 37 (1992) 1883.
[28] E. Morallon, A. Rodes, J.L. Vazquez, J.M. Perez, J. Electroanal. Chem. 391 (1995) 149.
[29] R. Ortiz, O.P. Marquez, J.C. Gutierrez, J. Phys. Chem. 100 (1996) 8389.
[30] M. Fleischmann, K. Korinck, D. Pletcher, J. Electroanal. Chem. 31 (1971) 39.
[31] S. Berchmans, H. Gomathi, G.P. Rao, J. Electroanal. Chem. 394 (1995) 267.
[32] M.A. Abdel Rahim, H.B. Hassan, R.M. Abdel Hamid, J. Power Source 154 (2006) 59.
[33] K.B. Kokoh, J.-M. Léger, B. Beden, C. Lamy, Electrochim. Acta 37 (1992) 1333.
[34] H. Yang, T. Lu, K. Xue, S. Sun, G. Lu, S. Chen, J. Mol. Catal. A: Chem. 144 (1999) 315.
[35] J.W. Kim, S.M. Park, J. Electrochem. Soc. 146 (1999) 1075.
[36] S.M.A. Shibli, V.S. Dilimon, J. Hydrogen Energy 32 (2007) 1694.
[37] B. Moreno, E. Chinarro, J.L.G. Fierro, J.R. Jurado, J. Power Source 169 (2007) 59.
[38] H. Song, X. Qiu, F. Li, W. Zhu, L. Chen, Electrochem. Commun. 9 (2007) 1298.
[39] S. Mehandru, A. Andreson, P. Ross, J. Catal. 100 (1986) 210.
[40] J. Michalski, T. Wejrzanowski, S. Gierlotka, J. Bielinski, K. Konopka, T. Kosmac, K.J.J. Kurzydlowski, Eur. Ceram. Soc. 27 (2007) 831.